

Article

# Influence of a Constant Perpendicular High Magnetic Field on the Electrodeposition of Calcium Phosphate Coating

Anne-Lise Daltin \*  and Jean-Paul Chopart 

Matériaux et Ingénierie Mécanique (MATIM), University of Reims Champagne Ardenne, CEDEX 2, 51687 Reims, France; jp.chopart@univ-reims.fr

\* Correspondence: anne-lise.daltin@univ-reims.fr; Tel.: +33-326918449

**Abstract:** Calcium phosphate coatings were formed on a Ti6Al4V substrate by electrodeposition under a high magnetic field up to 16 T. The magnetic field was parallelly applied to the vertical surface electrode. Changes in crystal morphology of calcium phosphates were investigated as a function of the magnetic field amplitude, and the results are discussed in terms of magnetic field effects. Magneto-hydrodynamic convection due to the Lorentz force could considerably reduce the formation of volcano-like structures and generate more uniform deposits without changing Ca/P ratios.

**Keywords:** calcium phosphate; crystal orientation; electrodeposition; hydroxyapatite; high magnetic field; magneto-electrodeposition; magneto-hydrodynamics; octacalcium phosphate

## 1. Introduction

Calcium phosphates (CaP) are biomaterials that are usually used as coatings of biometals for dental implants and prostheses [1]. There is interest in studying such materials because of their ability to chemically bond to bones. The calcium orthophosphates family constituents include hydroxyapatite (HAP,  $\text{Ca}_{10}(\text{PO}_4)_6(\text{OH})_2$ ) with a Ca-to-P ratio equal to 1.67 and octacalcium phosphate (OCP,  $\text{Ca}_8\text{H}_2(\text{PO}_4)_6 \cdot 5\text{H}_2\text{O}$ ) with a Ca-to-P ratio equal to 1.33. OCP has been confirmed as a bone substitute material that enhances bone regeneration [2]. Osteoconductivity can be improved if the synthetic hydroxyapatite is closer to that of a bone mineral in crystal structure, size, and morphology [3].

These coatings can be obtained by cathodic electrodeposition from aqueous solution and can be optimal by optimizing electrodeposition parameters, technological conditions, the adjusted current form [4], or by using simulated body fluid (SBF) as an electrolytic medium [5]. Numerous works concern the deposits of thin films on titanium substrates [6–10]. Electrodeposition has numerous advantages such as low temperature, high deposition rates, low cost, and allowing large-area deposition and complex shapes. However, electrochemical deposition generates nonuniform coatings due to the high production of  $\text{H}_2$  bubbles during the process. Some solutions have been proposed to overcome this problem such as electrodeposition under vacuum [8] or pulse electrodeposition [11] with an electrolytic bath containing  $\text{H}_2\text{O}_2$ . It is known that the desorption of hydrogen can be enhanced by the presence of a magnetic field [12]. On the other hand, it is well known that the superimposition of an external magnetic field can reduce the grain size of electrodeposited metallic materials.

The magnetic field effects on the electrodeposition are due to magneto-hydrodynamic (MHD) effects at the cathode–electrolyte interface (in the hydrodynamic layer) that modify electrochemical reactions [13,14], enhance mass transport, and change the electrode interfacial conditions such as surface pH and ionic adsorption. Such a modification can mainly be related to the Lorentz force when the magnetic field is perpendicular to the current density. Furthermore, these effects are a consequence of a micro-MHD flow (microscopic minute vortices that emerge inside the boundary layer) [15]. The electrodeposition of



**Citation:** Daltin, A.-L.; Chopart, J.-P. Influence of a Constant Perpendicular High Magnetic Field on the Electrodeposition of Calcium Phosphate Coating. *Magnetochemistry* **2022**, *8*, 62. <https://doi.org/10.3390/magnetochemistry8060062>

Academic Editor: Xuegeng Yang

Received: 19 May 2022

Accepted: 31 May 2022

Published: 7 June 2022

**Publisher's Note:** MDPI stays neutral with regard to jurisdictional claims in published maps and institutional affiliations.



**Copyright:** © 2022 by the authors. Licensee MDPI, Basel, Switzerland. This article is an open access article distributed under the terms and conditions of the Creative Commons Attribution (CC BY) license (<https://creativecommons.org/licenses/by/4.0/>).

calcium phosphate has already been studied in the presence of a magnetic field [16–19], but very few studies relate to the superimposition of an intense magnetic field apart from our own work, and not in the configuration where the magnetic field is applied parallel to the cathode electrode [20].

In this study, our purpose is to use a high magnetic field to generate magnetohydrodynamic convection (Lorentz force) to avoid the formation of such an inhomogeneity and to explore the influence of a high magnetic field on the morphology and composition of those coatings.

## 2. Materials and Methods

A calcium phosphate coating was performed on a 1 cm<sup>2</sup> circular embedded Ti6Al4V electrode after increasing its roughness using 50 mesh abrasive paper to promote the adhesion of the deposit. The titanium alloy used in these experiments was a Goodfellow Ti90/Al 6/V, whose analysis type was Al 6%, Fe 0.03%, V 4%, C 0.022%, H 0.01%, N 0.01%, O 0.065%, and Ti rest. The surface roughness of substrates before electrodeposition was measured with a SJ 301 Mitutoyo surface roughness tester and had a value of  $3.1 \pm 0.1$   $\mu\text{m}$ . Substrates were washed with ethanol and rinsed with distilled water. For the electrolytic deposition, a three-electrode cell with a Ti6Al4V vertical substrate as a working electrode (WE), Pt wire as a counter electrode, and Ag/AgCl as a reference electrode were used. The electrolytic solution was composed of 0.042 mol/L of Ca(NO<sub>3</sub>)<sub>2</sub>·4H<sub>2</sub>O, and 0.025 mol/L of NH<sub>4</sub>H<sub>2</sub>PO<sub>4</sub> (both analytical grade) in deionized water with a Ca/P ratio equal to 1.68 and a pH equal to  $4.5 \pm 0.1$ . All electrodeposition experiments were carried out in a double-walled 200 mL borosilicate glass cell for water circulation, which allowed us to work at an  $80 \pm 2$  °C temperature using a thermostatic bath. For the experiments under a magnetic field, a special cell was designed and built to fit into the  $\varnothing = 160$  mm room-temperature bore of a 20 T 20 MW resistive magnet (LNCMI). The corresponding experimental apparatus is schematized in Figure 1, where the glass cell was put into the gap of a 160 mm bore that could generate a vertical upward magnetic field up to 16 T, which was homogeneous on the whole cell. The electrode potential was maintained at  $-1.55$  V/<sub>AgAgCl</sub> with a potentiostat (PGZ 301, Tacussel-Radiometer Inc. Copenhagen) for 45 min while the current was followed by chronoamperometry. During these experiments, the potentiostat/galvanostat equipment was controlled by VoltaMaster-4 software. The surface topography of the coatings was determined with a 3D digital microscope (Keyence VHX-5000). The coating surface morphology was performed by scanning electron microscopy (SEM) using a JSM-6460LA microscope (Jeol) in secondary electron mode with an operating voltage of 25 kV at different magnifications ranging from  $8\times$  to  $10,000\times$ . The chemical compositions were obtained by energy-dispersive X-ray spectroscopy (EDS) at a working distance of 11 mm, considering the factors of atomic number Z, absorption A, and fluorescence correction F, in a ZAF matrix correction model. The X-ray diffraction (XRD) patterns were collected in the  $2\theta$  range of  $3\text{--}60^\circ$ , with a  $2\theta$  step of  $0.04^\circ$  and a counting time of 2 s by step, using a D8 advance Bruker diffractometer with Cu-K $\alpha$  radiation ( $\lambda = 1.54056$  Å) at 40 kV and 40 mA.

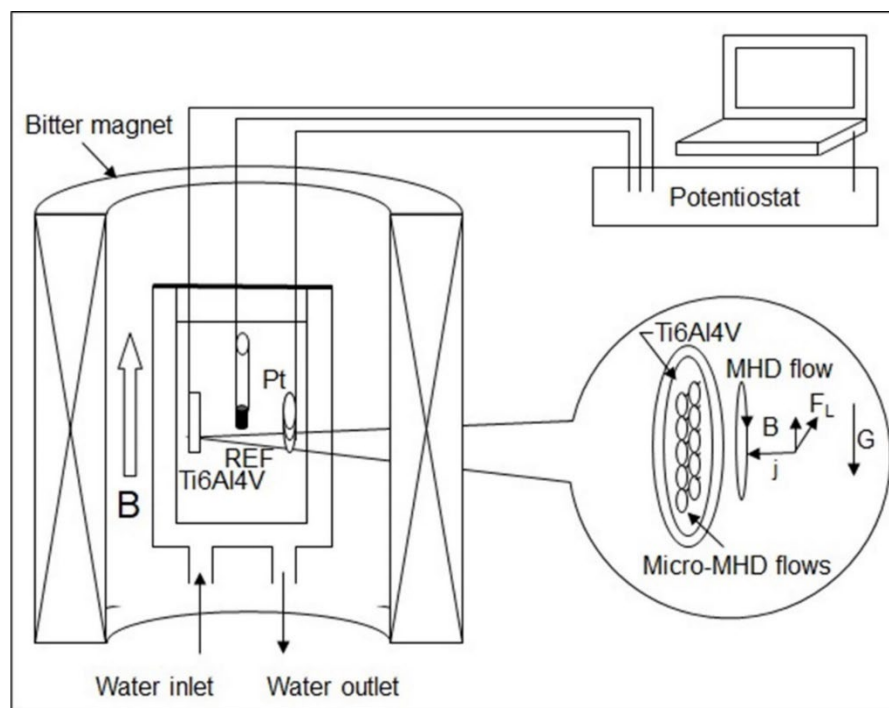
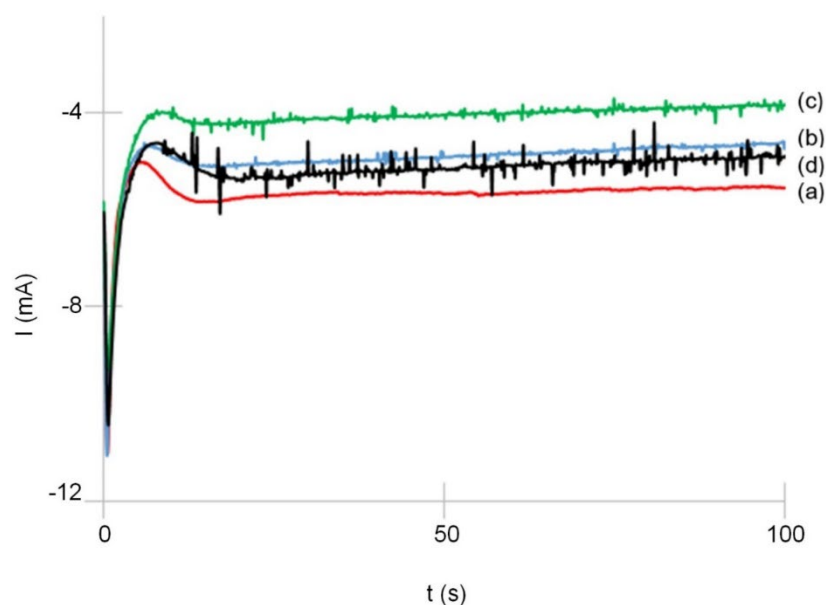


**Figure 1.** The schematic experimental apparatus.

### 3. Results and Discussion

#### 3.1. Analysis of Transient Curves

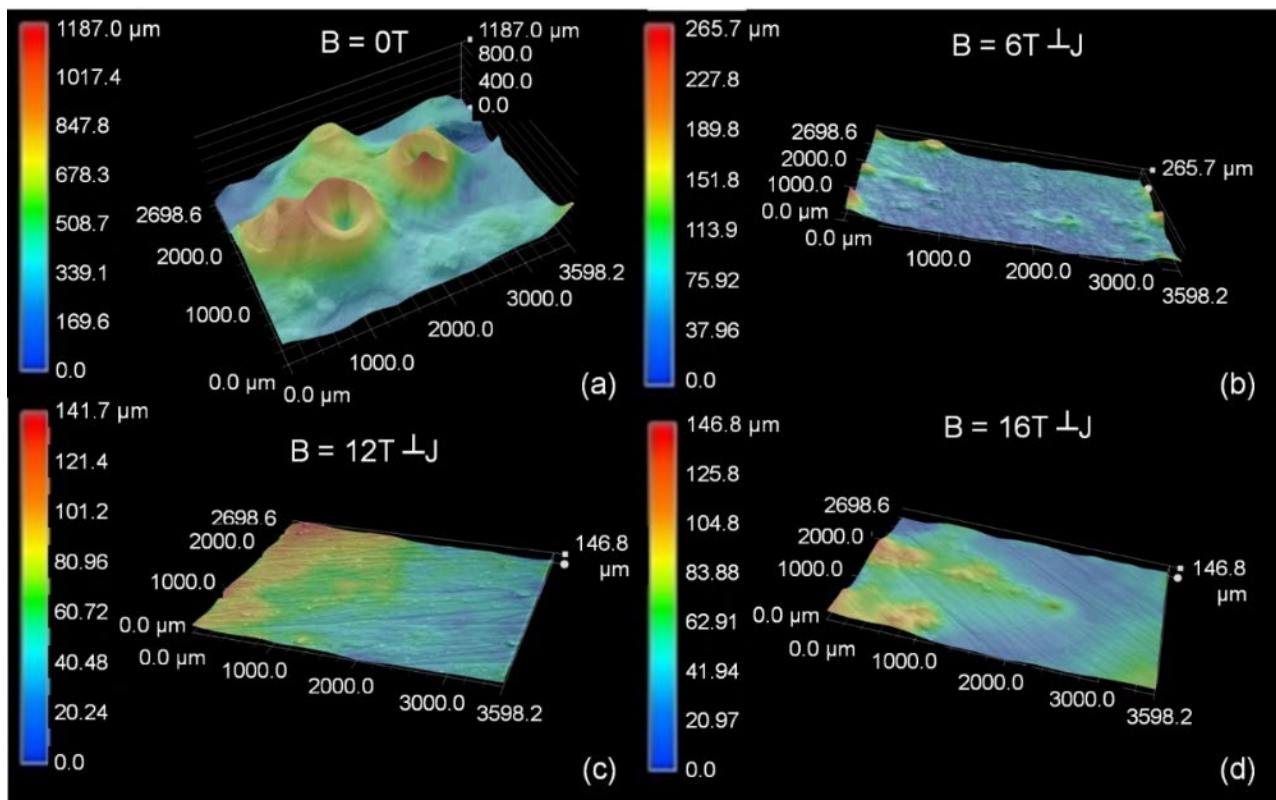
The current against time transients of CaP deposits under no magnetic field or different magnetic field amplitudes up to 16 T are shown in Figure 2. The examination of the transients reveals two points that can be noted: the first one is a slight decrease in the stationary current that can be observed when a high magnetic field is applied in the parallel configuration versus the surface electrode; the second one is the increase in noise with the magnetic field amplitude. The analysis of these current transient curves shows that no change in nucleation mode can be observed; indeed, the nucleation is progressive with or without the magnetic field.



**Figure 2.** Potentiostatic current transients for the deposition of CaP coatings at  $-1.55 \text{ V}/_{\text{AgAgCl}}$  under (a)  $B = 0 \text{ T}$ , (b)  $B = 6 \text{ T}^{\perp}\text{J}$ , (c)  $B = 12 \text{ T}^{\perp}\text{J}$ , and (d)  $16 \text{ T}^{\perp}\text{J}$ , during the first 50 s.

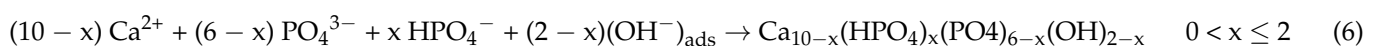
### 3.2. Surface Topography and Morphology

The surface topography of the coatings synthesized at different magnetic field amplitudes from 0 to 16 T (Figure 3) reveals the disappearance of craters in the presence of the field as it has already been shown in the case of a high magnetic field perpendicularly applied to the working electrode for different CaP coatings [20], while volcano-like structures are present without magnetic field superimposition, as it is shown in SEM images for low magnification in Figure 4(A1,A2). These volcano-like structures are zoomed in Figure 5A,B. The presence of these craters can be explained by the presence of hydrogen bubbles, as schematized in Figure 5C,D, and related to the reduction of H<sub>2</sub>O that generates H<sub>2</sub> molecules that coalesce in gaseous macroscopic bubbles, while the CaP compounds continue to grow around them.



**Figure 3.** Surface topography of calcium phosphate electrodeposited under (a)  $B = 0$  T, (b)  $B = 6$  T $\perp$ J, (c)  $B = 12$  T $\perp$ J, (d)  $B = 16$  T $\perp$ J.

Some electrochemical and chemical reactions could be involved in the electrocrystallization of calcium phosphate on the TA6V alloy such as:



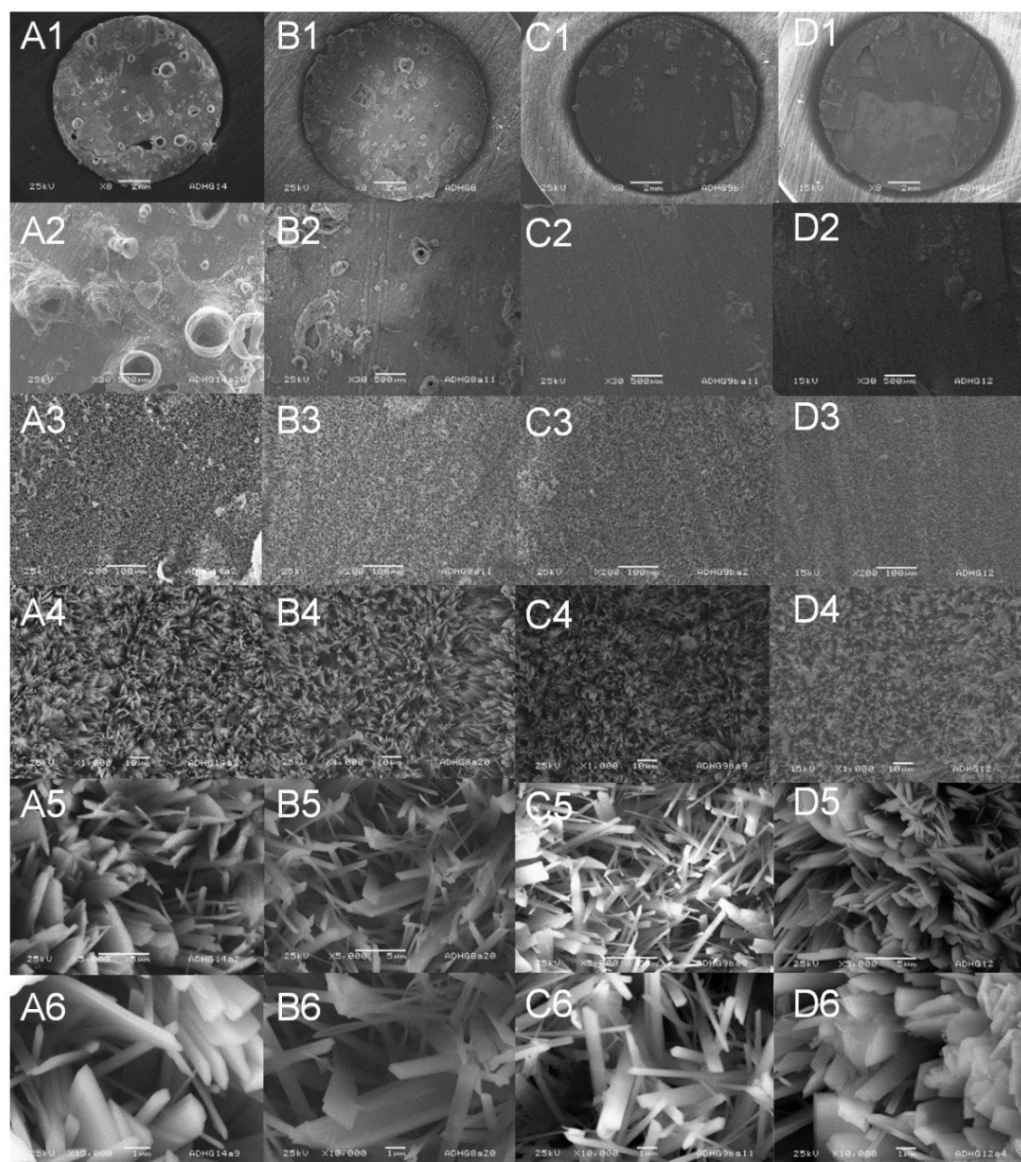


**Figure 4.** SEM images of calcium phosphate coatings electrodeposited at  $E = -1550 \text{ mV}/\text{AgAgCl}$  under different magnetic field amplitudes: (A1–A6)  $B = 0 \text{ T}$ , (B1–B6)  $B = 6 \text{ T} \perp J$ , (C1–C6)  $B = 12 \text{ T} \perp J$ , (D1–D6)  $B = 16 \text{ T} \perp J$ .

Reactions (1–2) lead to a local increase in pH within the diffusion layer and therefore allow reaction (3). The increase in the local pH at the interface of the titanium alloy and electrolyte will heighten the supersaturation of calcium phosphate and lead to the precipitation of various CaP phases on the cathode such as hydroxyapatite or octacalcium phosphate. At the same time, the reduction of  $\text{H}_2\text{O}$  occurs, generating  $\text{H}_2$  molecules that coalesce in gaseous macroscopic bubbles.

The magnetohydrodynamic convection due to the Lorentz force is the main cause of the disappearance of the craters, thanks to the accelerated desorption of hydrogen bubbles. The SEM image in Figure 4D1 shows that for the 16 T magnetic field amplitude, the coating is not adherent on the Ti6Al4V substrate. Furthermore, the coating morphology changes from belt-shaped crystallites in the absence of a magnetic field (Figure 4(A5,A6)) to needle-shaped crystallites under a 12 T magnetic field (Figure 4(C5,C6)). The crystallites obtained under a 16 T magnetic field amplitude are different and also have a needle-shaped (Figure 4(D5,D6)). Some similar changes in surface morphology, that is, from plate-like to

needle-like, have been shown by Seyedraoufi et al. [21] for HAP coatings electrodeposited on a Mg-Zn scaffold, in that case, with an increase in the current density.

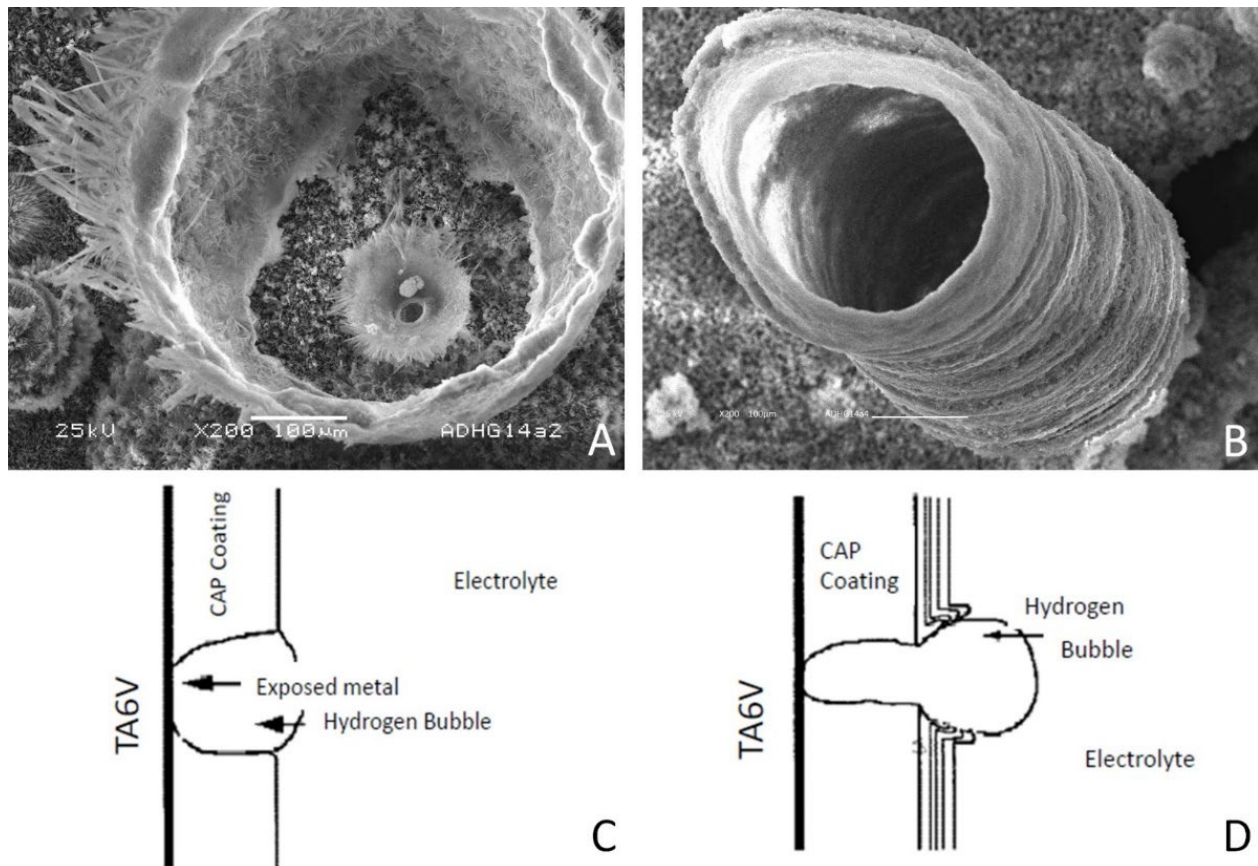


**Figure 5.** (A,B) SEM images and schematic of volcano-like craters built-up on calcium phosphate coatings that are electrodeposited at  $E = -1550 \text{ mV}/_{\text{AgAgCl}}$  under  $B = 0 \text{ T}$ . (C,D) Schematized hydrogen bubble evolution and craters formation.

### 3.3. X-ray Diffraction

Figure 6 shows the XRD patterns for the as-deposited coatings with no magnetic field applied and in the presence of a magnetic field parallel to the cathode surface.

The present crystallographic phases are identified in the absence of a magnetic field and for several magnetic field amplitudes up to 16 T. The presence of both OCP (JCPDS-ICDD No. 01-079-423) and HAP (JCPDS-ICDD No. 00-09-432) is identified. The peaks at  $2\theta = 4.7^\circ$  corresponding to the OCP (100) plane are always the most intense peaks. This confirms the presence of OCP in large quantities under all conditions: with and without the superimposition of a high magnetic field. As shown in Figure 7a, the intensity of the HAP (110) peak increases with the magnetic field showing the preferential growth of these planes with the MHD convection. The growth of Ca-P crystals is a time-dependent process and is markedly affected by the degree of supersaturation of the electrolyte [10]. The MHD convection may alter the diffusion of calcium, phosphate, and hydroxyl ions to the different HAP crystals surface. The HAP compounds have a hexagonal crystal structure characterized by the space group  $P6_3/m$ . The HAP unit cell has rich phosphate and hydroxyl ions at the c-plane, which makes this plane negatively charged and the calcium ions at the a-plane therefore positively charged. By modifying the degree of supersaturation with the magnetization force, there is the formation of crystallites with higher surface-energy faces. With a high magnetic field, when  $j$  is perpendicular to  $B$ , the Lorentz force arises, and it is greater on the tips of the crystallite [22]. This fact generates a zone of high concentration that permits a faster growth in the c-axis direction. As the

crystallites are flexible, the surface with the (110) plane is more exposed to X-rays and the XRD measurement shows an increase in the (110) peak intensity with the the magnetic field amplitude. In the same way, the shape of crystallites changes from the belt to the needle-shaped one.

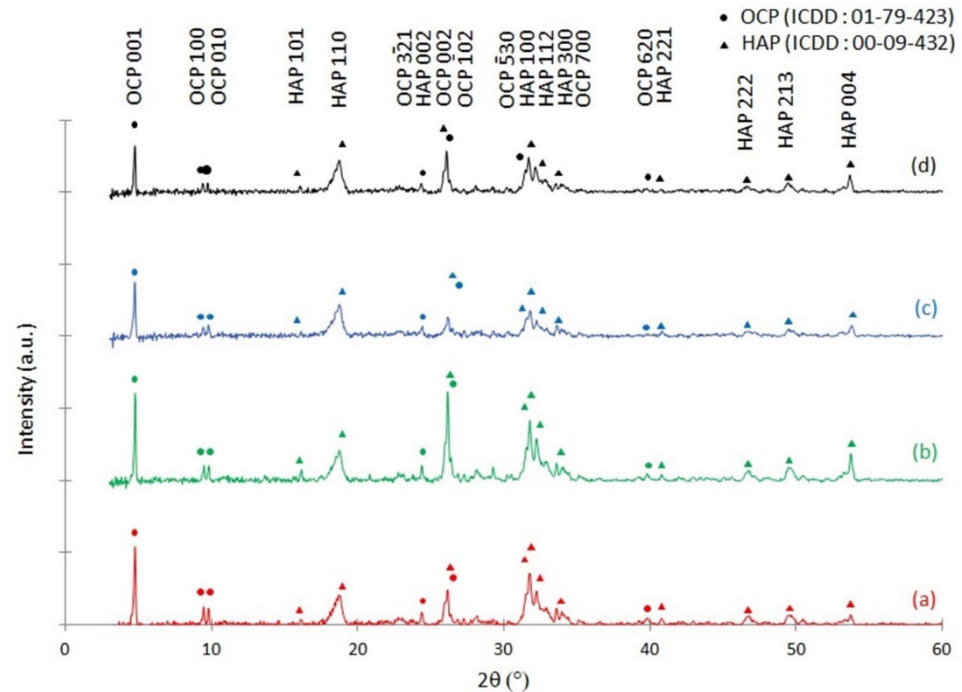


**Figure 6.** XRD patterns of calcium phosphate coatings products obtained with various magnetic fields superimposed: (a)  $B = 0$  T, (b)  $B = 6$  T $\perp$ J, (c)  $B = 12$  T $\perp$ J, (d)  $B = 16$  T $\perp$ J. Dot (●) corresponds to OCP reflections peaks; triangle (▲) corresponds to HAP reflections peaks.

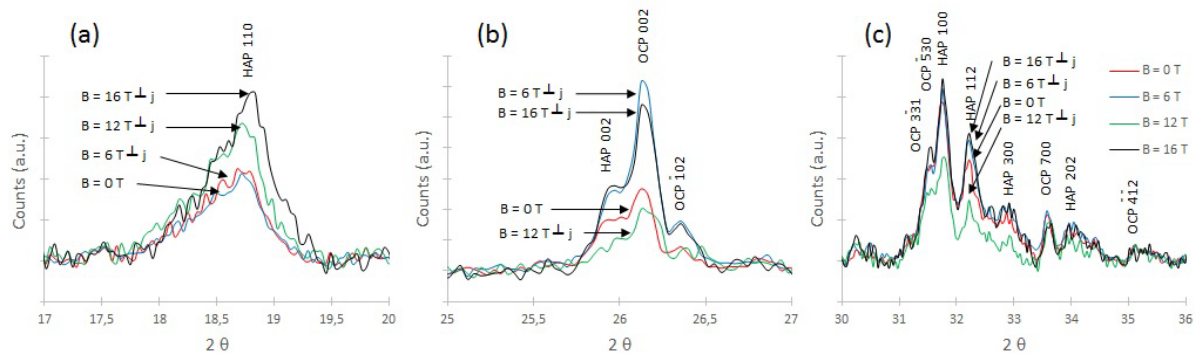


**Figure 7.** XRD patterns of calcium phosphate coatings products with relative intensities obtained when normalized to the most intense peak (OCP (100) at  $2\theta = 4.7^\circ$ ) between (a)  $2\theta = 17^\circ$  and  $2\theta = 20^\circ$ , (b)  $2\theta = 25^\circ$  and  $2\theta = 27^\circ$ , and (c)  $2\theta = 30^\circ$  and  $2\theta = 36^\circ$ .

The micro-MHD convection on the crystallite edges can also modify growth and, therefore, the morphology of the Ca-P coating can be tuned to a belt-shaped one to needle-like one.

Such calcium phosphates biomaterials are commonly used as coatings of titanium alloys for dental implants and prostheses. For this, it is interesting to remark that coatings are composed of a mixture of OCP and HAP. OCP has been regarded as the precursor of biological apatite HAP and has a positive role in osteoconduction and osteoinduction because it is more resorbable and it enhances more bone formation than HAP does [23].

### 3.4. Chemical Composition

The Ca/P ratios of the coatings electrodeposited with the superimposition of different magnetic fields are estimated by EDS and are, respectively,  $\text{Ca/P} = 1.74 \pm 0.02$ ,  $\text{Ca/P} = 1.70 \pm 0.04$ ,  $\text{Ca/P} = 1.72 \pm 0.01$ , and  $\text{Ca/P} = 1.64 \pm 0.04$  for 0 T, 6 T, 12 T, and 16 T. There are no significant changes in these values that are also representative of a mixture of OCP and HAP, as shown with the XRD analyses.

## 4. Conclusions

The magnetohydrodynamic convection used during the potentiostatic deposition of calcium phosphate coatings can significantly reduce the formation of volcano-like structures and generate more uniform deposits without changing Ca/P ratios. The desorption of hydrogen is enhanced by the magnetic field superimposition during the electrodeposition process. The magnetohydrodynamic convection due to the Lorentz force is the main cause of the disappearance of the craters, but for the highest magnetic field amplitude (16 T), the coating is not adherent on the Ti6Al4V substrate. No change in Ca/P composition is obtained with magnetic field superimposition, while the preferential orientation of HAP (110) is enhanced. The coating morphology changes from belt-shaped crystallites in the absence of a magnetic field to needle-shaped crystallites under a 12 T magnetic field. The high magnetic field is an in situ method that controls the electrodeposition process over a large surface area with good opportunities. In addition, annealing under a high magnetic field could be another way to obtain coating materials with higher characteristics [24].

**Author Contributions:** Conceptualization, A.-L.D. and J.-P.C.; methodology, formal analysis, investigation, writing—original draft preparation, writing—review and editing, A.-L.D.; project administration, J.-P.C. All authors have read and agreed to the published version of the manuscript.

**Funding:** This research received no external funding.

**Informed Consent Statement:** Not applicable.

**Data Availability Statement:** Not applicable.

**Acknowledgments:** We acknowledge the support of the LNCMI-CNRS, member of the European Magnetic Field Laboratory (EMFL).

**Conflicts of Interest:** The authors declare no conflict of interest.

## References

1. Dorozhkin, S.V. Calcium Orthophosphates as Bioceramics: State of the Art. *J. Funct. Biomater.* **2010**, *1*, 22–107. [[CrossRef](#)] [[PubMed](#)]
2. Suzuki, O.; Kamakura, S.; Katagiri, T.; Nakamura, M.; Zhao, B.; Honda, Y.; Kamijo, R. Bone formation enhanced by implanted octacalcium phosphate involving conversion into Ca—Deficient hydroxyapatite. *Biomaterials* **2006**, *27*, 2671–2681. [[CrossRef](#)] [[PubMed](#)]
3. Narayanan, R.; Kwon, T.Y.; Kim, K.H. Direct nanocrystalline hydroxyapatite formation on titanium from ultrasonated electrochemical bath at physiological pH. *Mater. Sci. Eng. C* **2008**, *28*, 1265–1270. [[CrossRef](#)]
4. Li, T.T.; Ling, L.; Lin, M.C.; Peng, H.K.; Ren, H.T.; Lou, C.W.; Lin, J.H. Recent advances in multifunctional hydroxyapatite coating by electrochemical deposition. *J. Mater. Sci.* **2020**, *55*, 6352–6374. [[CrossRef](#)]
5. Uribe, R.; Uvillus, A.; Fernandez, L.; Bonilla, O.; Jara, A.; Gonzales, G. Electrochemical Deposition of Hydroxyapatite on Stainless Steel Coated with Tantalum/Tantalum Nitride Using Simulated Body Fluid as an Electrolytic Medium. *Coatings* **2022**, *12*, 440. [[CrossRef](#)]
6. Abdel-Aal, E.A.; Dietrich, D.; Steinhäuser, S.; Wielage, B. Electrocrystallization of nanocrystallite calcium phosphate coatings on titanium substrate at different current densities. *Surf. Coat. Technol.* **2008**, *202*, 5895–5900. [[CrossRef](#)]
7. Blackwood, D.J.; Seah, K.H.W. Electrochemical cathodic deposition of hydroxyapatite: Improvements in adhesion and crystallinity. *Mater. Sci. Eng. C* **2009**, *29*, 1233–1238. [[CrossRef](#)]
8. Popa, M.V.; Moreno, J.M.C.; Popa, M.; Vasilescu, E.; Drob, P.; Vasilescu, C.; Drob, S.I.J.S.; Technology, C. Electrochemical deposition of bioactive coatings on Ti and Ti–6Al–4V surfaces. *Surf. Coat. Technol.* **2011**, *205*, 4776–4783. [[CrossRef](#)]
9. Wang, S.H.; Shih, W.J.; Li, W.L.; Hon, M.H.; Wang, M.C. Morphology of calcium phosphate coatings deposited on a Ti–6Al–4V substrate by an electrolytic method under 80 Torr. *J. Europ. Ceram. Soc.* **2005**, *25*, 3287–3292. [[CrossRef](#)]

10. Mokabber, T.; Lu, L.Q.; Van Rijn, P.; Vakis, A.I.; Pei, Y.T. Crystal growth mechanism of calcium phosphate coatings on titanium by electrochemical deposition. *Surf. Coat. Technol.* **2018**, *334*, 526–535. [[CrossRef](#)]
11. Drevet, R.; Benhayoune, H.; Wortham, L.; Potiron, S.; Douglade, J.; Laurent-Maquin, D. Effects of pulsed current and H<sub>2</sub>O<sub>2</sub> amount on the composition of electrodeposited calcium phosphate coatings. *Mater. Charact.* **2010**, *61*, 786–795. [[CrossRef](#)]
12. Chopart, J.P.; Aaboubi, O.; Msellak, K. Electrochemical characterization of Ni-Fe alloy codeposition under MHD control. *J. Solid State Electrochem.* **2007**, *11*, 703–710. [[CrossRef](#)]
13. Aogaki, R.; Fueki, K.; Mukaibo, T. Application of Magnetohydrodynamic Effect to the Analysis of Electrochemical Reactions -1. MHD Flow of an Electrolyte Solution in an Electrode-Cell with a Short Rectangular Channel. *Denki Kagaku (Presently Electrochem.)* **1975**, *43*, 504–508. [[CrossRef](#)]
14. Aogaki, R.; Morimoto, R.; Asanuma, M. Nonequilibrium fluctuations in micro-MHD effects on electrodeposition. *J. Magn. Magn. Mater.* **2010**, *322*, 1664–1668. [[CrossRef](#)]
15. Daltin, A.L.; Baudart, P.; Debray, F.P.; Chopart, J.P. Morphology change of electrodeposited calcium phosphate coating on Ti6Al4V substrate under high magnetic field. *J. Iron Steel Res. Int.* **2012**, *19*, 1162–1165.
16. Tohidi, P.M.; Safavi, M.S.; Etminanfar, M.; Khalil-Allafi, J. Pulsed electrodeposition of compact, corrosion resistant, and bioactive HAp coatings by application of optimized magnetic field. *Mater. Chem. Phys.* **2020**, *254*, 123511. [[CrossRef](#)]
17. Liu, C.; Tian, A.; Yang, H.; Xu, Q.; Xue, X. Electrodeposited hydroxyapatite coatings on the TiO<sub>2</sub> nanotube in static magnetic field. *Appl. Surf. Sci.* **2013**, *287*, 218–222. [[CrossRef](#)]
18. Zhao, X.N.; Li, H.J.; Li, K.Z.; Lu, J.H.; Zhang, L.L.; Cao, S. Electrodeposition of nanostructured calcium phosphate coating under magnetic field. *Mater. Technol.* **2012**, *27*, 371–374. [[CrossRef](#)]
19. Tian, A.; Xue, X.; Liu, C.; He, J.; Yang, Z. Electrodeposited hydroxyapatite coatings in static magnetic field. *Mater. Lett.* **2010**, *64*, 1197–1199. [[CrossRef](#)]
20. Daltin, A.L.; Ahmed Chekkat, A.; Millet, P.; Chopart, J.P. Electrocrystallization kinetics of hydroxyapatite and calcium phosphate coatings under magnetic field. *Magnetohydrodynamics* **2012**, *48*, 261–270.
21. Seyedraoufi, Z.; Mirdamadi, S. Effects of pulse electrodeposition parameters and alkali treatment on the properties of nanohydroxyapatite coating on porous Mg–Zn scaffold for bone tissue engineering application. *Mater. Chem. Phys.* **2014**, *148*, 519–527. [[CrossRef](#)]
22. Daltin, A.L.; Chopart, J.P. Morphology of magneto-electrodeposited Cu<sub>2</sub>O microcrystals. *CrystEngComm* **2011**, *13*, 3373–3377. [[CrossRef](#)]
23. Habibovic, P.; van der Valk, C.M.; van Blitterswijk, C.A.; De Groot, K.; Meijer, G. Influence of octacalcium phosphate coating on osteoinductive properties of biomaterials. *J. Mater. Sci. Mater. Med.* **2004**, *15*, 373–380. [[CrossRef](#)]
24. Li, D.; Gao, Y.; Wang, Q.; Li, G.; Wu, C.; Daltin, A.L.; Chopart, J.P. Tailoring the morphology, structure and magnetic properties of electrodeposited CoFe films onto Si(100) by in-situ uniform and gradient high magnetic fields. *J. Electrochem. Soc.* **2016**, *163*, D836–D841. [[CrossRef](#)]